International Journal of Fluid Power 4 (2003) No. 1 pp. 49-57

PNEUMATIC LANDSLIDE GENERATOR

Hermann M. Fritz[1] and Peter Moser[2]

[1]*Laboratory of Hydraulics, Hydrology and Glaciology (VAW), Swiss Federal Institute of Technology (ETH), CH-8092 Zurich, Switzerland*
Georgia Institute of Technology – GTREP, 6001 Chatham Center Drive, Suite 350, Savannah, Ga 31405, USA (current)
hermann.fritz@gtrep.gatech.edu
[2]*Festo AG, Moosmattstrasse 24, CH-8953 Dietikon, Switzerland*
peter_moser@festo.ch

Abstract

A pneumatic landslide generator was developed specifically for the investigation of landslide generated impulse waves in reservoirs, lakes, bays or oceans in a two-dimensional physical laboratory model. The landslides were successfully modelled with an artificial granulate. The pneumatic landslide generator was designed to control the slide impact characteristics and enable exact reproduction and independent variation of single dynamic slide parameters. The two pneumatic linear drives catapulted the landslides to velocities up to 7.3 m/s on an acceleration distance of less than 0.9 m. The operation of linear drives 3.6 times beyond their certified velocity range is highlighted. Total masses of up to 174 kg were accelerated. The slotted cylinders enabled a compact mechanical design and a stroke length equal to 70 % of the overall cylinder length. The pneumatic deceleration by temporary airflow and pressure gradient reversal is presented. Real time valve response problems in high-speed applications are discussed and solved with preset trigger signals programmed to the pneumatics control unit. The behaviour of the whole pneumatic system was successfully simulated with the computer aided cylinder optimisation system software (CACOS). The measurements and numerical simulations are compared.

Keywords: pneumatic linear drives, slotted cylinders, high-speed application, large moving mass, airflow reversal, pneumatic deceleration, external shock absorber, real time problems, CACOS numerical simulation, landslide impacts, impulse waves

Introduction

Large water waves in reservoirs, lakes, bays and oceans may be generated by landslides, shore instabilities, snow avalanches, glacier and rock falls (Slingerland and Voight, 1979). The resulting impulse waves can cause disaster due to run-up along the shoreline and overtopping of dams (Vischer and Hager, 1998). Landslide generated impulse waves were investigated in physical model experiments based on Froude similarity with state-of-the-art laser measurement techniques such as digital particle image velocimetry (PIV) and laser distance sensors (Fritz, 2002a). The physical model results were compared to the giant rockslide generated impulse wave, which struck the shores of the Lituya Bay, Alaska, in 1958. The measurements obtained in the physical model were in agreement with the in-situ data (Fritz et al, 2001).

This manuscript was received on 13 September 2002 and was accepted after revision for publication on 27 January 2003

The granular rockslide impact experiments were conducted in a rectangular prismatic water wave channel, which was 11 m long, 0.5 m wide and 1 m deep. At the front end of the channel a 3 m long hill slope ramp was built into the channel. The hill slope angle α was variable from 30° to 90°, but only the angle α = 45° was considered in the present study (Fritz, 2002b). The pneumatic landslide generator was built into the framework on the hill slope ramp shown in Fig. 1a. A gear drive allowed moving the whole landslide generator within roughly 1 m along the ramp to adapt its position to varying stillwater depths h and hill slope angles α. The slide box end position was always located at a distance of 0.7 m from the stillwater surface to avoid submergence of the sensitive pneumatic components during experiments. The pneumatic landslide generator is shown during a slide impact and wave generation experiment in Fig. 1b. The pneumatic landslide generator enabled starting the experiments with controlled

initial conditions just before impact, thus allowing exact reproduction and independent variation of single dynamic slide parameters. In particular different slide impact shapes were produced for the same slide impact velocity and mass.

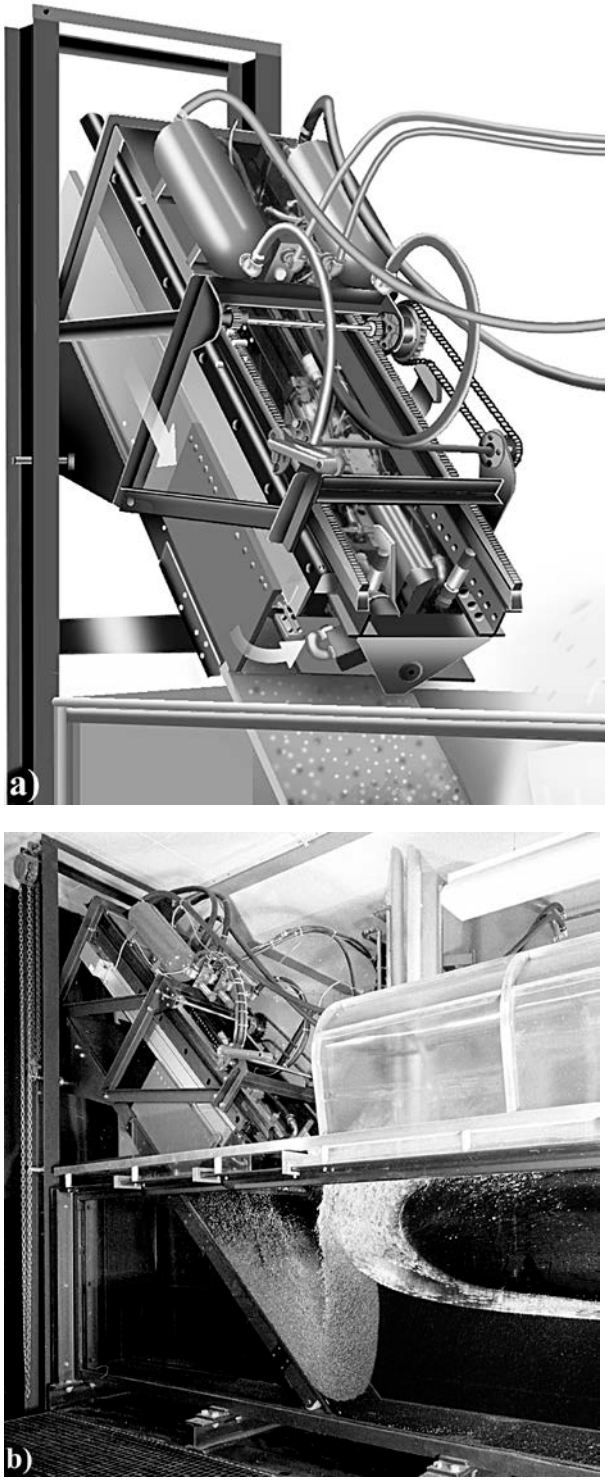

Fig. 1: *Pneumatic landslide generator: a) operation scheme with flap opening during slide box acceleration and slide release by box deceleration; b) slide impact experiment with v_B = 4 m/s, m_s = 108 kg, h = 0.45 m and α = 45° after slide release with the slide box in the end position*

2 Pneumatic Acceleration Mechanism

The pneumatic acceleration mechanism consisted of two double acting pneumatic linear drives, the slide box and the box opening mechanism. The two double acting pneumatic linear drives formed the main propulsion unit. The rod less pistons with slotted cylinders were preferred to standard un-slotted cylinders in combination with pistons with a rod due to space limitations. The rod less pistons had a diameter of 80 mm. The longitudinally slotted cylinder design allowed a maximum stroke of 1.25 m on a fixed total length of 1.77 m. The pneumatic acceleration mechanism is shown in Fig. 2 prior to the installation into the framework on the hill slope ramp. The landslide material was filled into the box from behind. The box opening mechanism for controlled landslide release consisted of a pneumatic cylinder driven flap. The box was mounted onto the linear guides with ball bearing units designed for high-speed motion.

Fig. 2: *Pneumatic slide acceleration mechanism with the two double acting pneumatic linear drives, the plain bearing guides, the slide box and the pneumatic cylinder driven flap opening mechanism*

The pneumatic acceleration mechanism was developed to release slides with masses 27 kg $\leq m_s \leq$ 108 kg and velocities 3 m/s $\leq v_s \leq$ 7 m/s. The application ranges of pneumatic linear drives with various cylinder diameters are shown in Fig. 3a. The dimensioning parameters are the maximum piston velocity v_p and the moving mass. The moving mass consisted of the slide mass m_s and the dead weight m_m = 66 kg of accelerated mechanical parts. The piston velocities in standard industrial applications are limited to $\leq$ 2 m/s. The velocity range covered in the experiments is well beyond the application range of the largest commercially available linear drives with 80 mm diameter. In particular, the armored sealing strips were considered critical components in slotted cylinders regarding high-speed applications. Hence intensive prototype testing and several modifications of the custom built pneumatic system were necessary regarding both hard- and software components. The modifications to the slotted cylinders were limited to both heads. The internal end-position cushioning was removed and the bore diameter in the head plates was increased to connect with 19.1 mm tubes. The linear drives performed flawless but the number of cycles after four years was still smaller

than 10000. The behaviour over millions of cycles typical for industrial applications remains untested. A cross-section of the whole pneumatic acceleration mechanism with the slotted cylinders, the linear bearing guides, the slide box and the flap opening mechanism is shown in Fig. 3b.

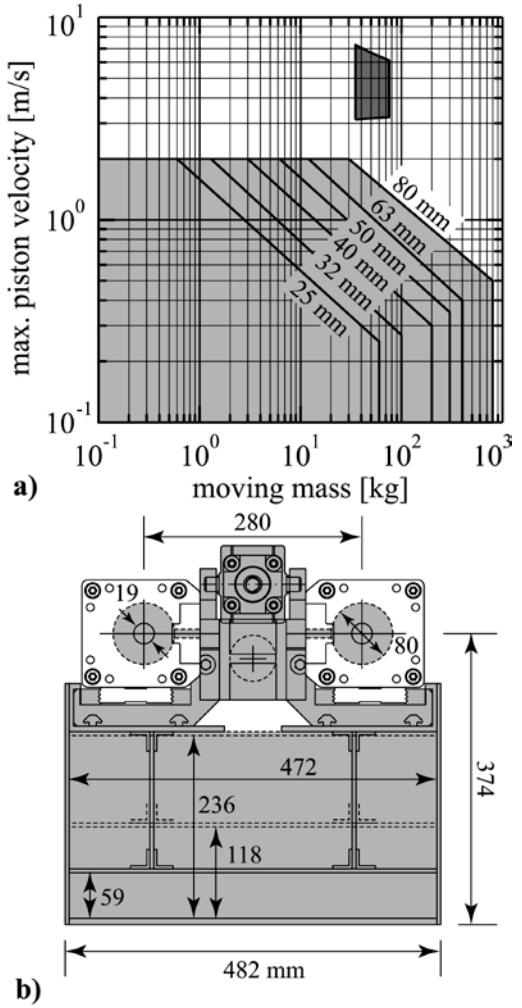

Fig. 3: *a) Application range of pneumatic linear drives with slotted cylinders with (colour) standard application range and (colour) experimental range; b) cross-section of the pneumatic acceleration mechanism with (colour) moving parts*

3 Slide Box

The landslides were modelled with an artificial granular material (PP-$BaSO_4$) consisting of 87 % barium-sulphate compounded with 13 % polypropylene (figures in weight percentage). The cylindrical grains with a mono-disperse grain diameter d_g = 4 mm are shown in Fig. 4a). Polypropylene (ρ = 0.91 t/m^3) was compounded with barium sulphate (ρ = 4.5 t/m^3) to reach the grain density ρ_g = 2.64 t/m^3, which matches common natural rock formations such as granite, limestone, sandstone and basalt. Natural rock densities vary roughly within 2 – 3.1 t/m^3 with a concentration around 2.6 – 2.7 t/m^3 (De Quervain, 1980; Kündig et al, 1997). As a bulk granular medium the density is reduced to the slide density ρ_s = 1.62 t/m^3 due to the porosity n = 39 % according to $\rho_s = (1 - n)\,\rho_g$. The estimated values for the slide density and porosity correspond to the granulate packing in the slide box. The granulate packing in the slide box is random and may be somewhere in between the densest and the loosest packing. The assumed porosity corresponds to data from granular Alpine debris flows (Tognacca, 1999) and the disturbed debris deposits at Mount St. Helens (Glicken, 1996).

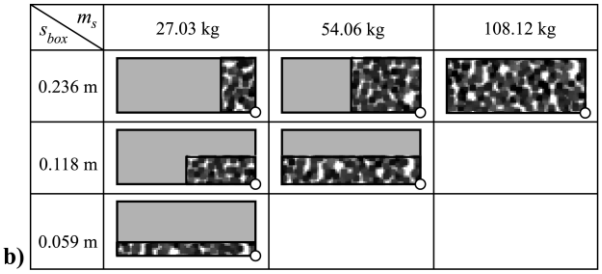

Fig. 4: *a) Landslide material: PP-BaSO4 granulate with grain diameter d_g = 4 mm, grain density ρ_g = 2.64 t/m^3, porosity n = 39 % and slide density ρ_s = 1.62 t/m^3; b) initial slide shapes and masses filled into the variable volume of the slide box confined by the positioning of the top and back plates; (○) slide front on hill slope ramp*

The granular slides were filled into the slide box with a maximum inner volume of 0.0668 m^3. The inner box width was fixed to 0.472 m. The inner box height s_{box} was reducible from 0.236 m to 0.118 m and 0.059 m by altering the position of the top plate. The three different positions of the top plate are shown in Fig. 3b. The inner box length was reducible from 0.6 m to 0.3 m and 0.15 m by altering the position of the back plate. The considered combinations of slide masses and initial slide shapes are shown in Fig. 4b. The slide mass and shape affect the performance of the pneumatic landslide generator by the accelerated mass and eccentricity of the load relative to the piston axis. Prior to box filling the slide mass m_s was measured to an accuracy of ±0.01 kg with a precision balance. The slide mass accuracy after box filling may be estimated to ±0.05 kg.

4 Pneumatic Set-up

The pneumatic set-up consisted of two separate circuits for the flap opening and slide box motion. The

circuit with the two pneumatic linear drives was tuned for maximum slide box acceleration and peak velocity. The dynamics of the piston motion primarily depend on the pressure difference between the two cylinder chambers and the duration of the pressure difference build-up (Ohmer, 1994). Placing a 3-way solenoid valve directly on each cylinder end – rather than a sole 5-way

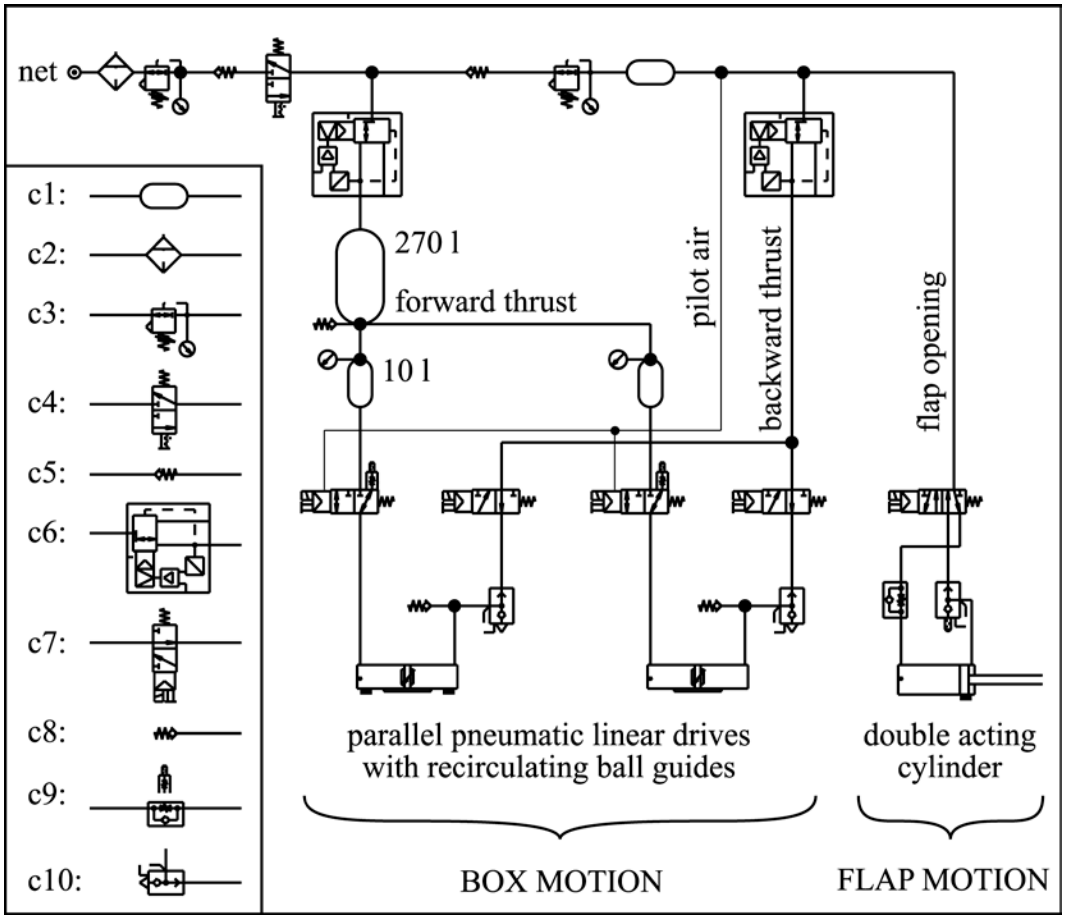

Fig. 5: *Pneumatic scheme with the circuits for the flap and the box motion with separate branches for the forward and backward thrusts and the symbols: c1) compressed air reservoir, c2) filter, c3) regulator, c4) start-up valve, c5) non-return valve, c6) precision proportional pressure regulator, c7) solenoid valve, c8) mechanical over-pressure exhaust valve, c9) exhaust flow control valve, c10) rapid exhaust valve*

valve for each cylinder – in combination with rapid exhaust valves placed directly on the exhaust side of the cylinders minimized the duration of the pressure difference build-up and allowed individual control. The pneumatic scheme with the circuits for the flap and the box motion with separate branches for the forward and backward thrusts is shown in Fig. 5.

The design of the pneumatic acceleration mechanism required a symmetric pressure difference build-up in the two parallel linear drives. The switching times of several 3-way solenoid valves were compared beforehand and those with matching behaviours selected. The necessary air discharge from the net to the linear drives was ensured with the determined inner diameter of 19.1 mm for all pneumatic components and tubes. Nevertheless a large 0.27 m^3 air reservoir was necessary to avoid a significant pressure drop in the ventilation chambers of the linear drives during the slide box acceleration. The mechanical over-pressure valves on the deceleration side of the linear drives limit pressure peaks to 12 bar in the exhaust chambers on the last section of the piston motion during the deceleration of the slide box, whereas the over-pressure valve connected to the reservoir was necessary only due to safety requirements.

5 Operation Principle

The pneumatic drives pushed the slide box down the ramp with an acceleration > g. The flap opened during box acceleration. The flap opening was programmed to begin as late as possible but still to get the flap open before box deceleration. The slide was released by the box deceleration. The box was decelerated with pneumatic pressure reversal – injecting bursts of compressed air at the lower end and exhausting at the upper end of the cylinders. The pneumatic deceleration by airflow and pressure gradient reversal was not capable to dissipate the kinetic energy completely. The remaining energy was absorbed by a custom built progressive shock absorber (Enidine Inc.). The external shock absorber was damaged once during preliminary testing due to an unsteady deceleration with destructive peaks. The high energies, which were absorbed in this single stroke

application, may damage hydraulic shock absorbers at higher repetition rates due to thermal effects. The different phases a landslide generation with the pneumatic acceleration mechanism are shown in Fig. 6. The high-speed piston and slide box motion is divided into three phases:

- Phase 1: Pneumatic acceleration driven by the governing pressure difference between the two piston sides. Flap opening.
- Phase 2: Pneumatic deceleration induced by the airflow and pressure gradient reversals prior to the impact on the external hydraulic shock absorber.
- Phase 3: Hydraulic dissipation of the remaining kinetic energy by the external shock absorber. Exhaustion at both cylinder ends.

Sauer (1996) made a similar phase distinction regarding a different high-speed application. The pneumatic landslide generator consumed a large amount of compressed air, while the actuators were running due to multiple exhaustions. The presented machine was only operated at low repetition rates – an experiment every few hours. Hence energy consumption was not critical in this application but may become crucial at higher repetition rates.

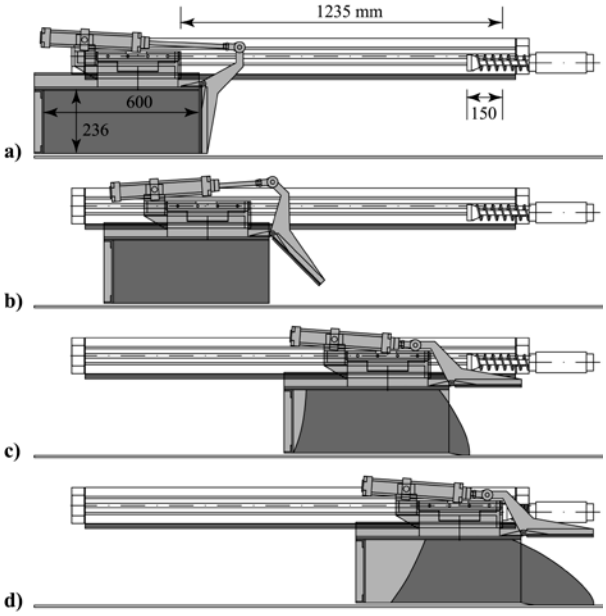

Fig. 6: *Slide box motion phases: a) initial position; b) slide box acceleration and flap opening, c) pneumatic deceleration by airflow and pressure gradient reversals; d) end position after hydraulic deceleration by the external shock absorber; with (■ colour) moving parts and (■ colour) granular slide*

Real time problems posed a major challenge to the operation of the pneumatic system. The crucial flap opening and box deceleration were not controlled with proximity switches due to the response time of the solenoid valves and the various operating pressures. The box and the flap had a response time of roughly 40 ms, which corresponds to box travel distance of 0.12 and 0.29 m at the minimum and maximum box velocities of 3 and 7.3 m/s, respectively. Therefore the pneumatic system was controlled with preset trigger signals. Prior to each experiment the trigger settings were determined and programmed to the control unit. The response of the system to the various commands is shown in Fig. 7c. A cross-section and a longitudinal cut of a slotted cylinder are shown in Fig. 7a and 7b, respectively. The notation is shown in Fig. 7b. In the initial position before the start at the starting time t_{01} the acceleration pressure was $p_a = 0$ bar. A zero pressure corresponds to the atmospheric pressure according to the pneumatic convention. The initial deceleration pressure $p_d = 1.3$ bar was necessary to hold the loaded slide box in the starting position. The control signals were sent to the valves at the starting time t_{01}. The valve switching was complete at the time t_{02} and the pressure gradient was starting to build up increasing the acceleration pressure p_a and reducing the initial deceleration pressure p_d. The slide box acceleration spanned from the time t_{02} to the time t_3. The maximum box velocity v_B was reached at the time t_3 with zero pressure gradient $p_a = p_d$. The slide release was initiated at the time t_3 with the maximum box velocity v_B reached during a stroke. Hence the flap had to be open at the time t_3. The flap trigger signal was set accordingly at the time t_{11}, the flap opening actually initiated at the time t_{12} and the flap was open at the time t_3. The valves at both cylinder ends were switched at the time t_{21} and the airflow reversal actually initiated at t_{22}. The slide box was decelerated pneumatically by the reversed pressure gradient $p_a < p_d$ for time $t > t_3$. Exhausting at the upper end of the cylinders reduced the driving force. Simultaneous ventilation at the lower end of the cylinders actively decelerated. Air was injected only over a short time period of a few tens of milliseconds before exhausting again. The exhaust trigger was set at the time t_{41}, the exhaustion and reduction of the deceleration pressure p_d began at the time t_{42} avoiding a piston motion in the negative x-direction. The time t_{42} corresponds to the impact on the external shock absorber. The slide box was in the end position at the time t_5. In the meantime both chambers were exhausted and the pressures reduced to the atmospheric pressure $p_a = p_d = 0$ bar.

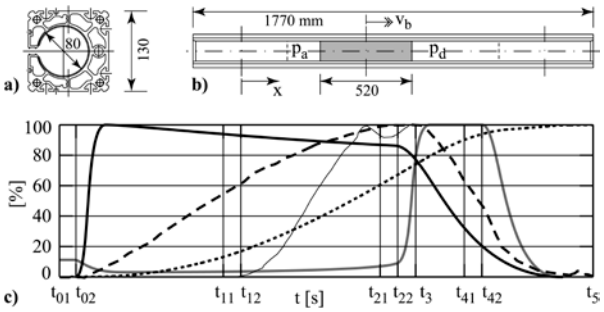

Fig. 7: *a) slotted cylinder cross-section; b) longitudinal cut of slotted cylinder and notation; c) operation principle with (——) acceleration pressure p_a, (——) deceleration pressure p_d, (– –) slide box velocity v_b, (····) slide box position x, (——) flap opening, t_{01} start trigger, t_{02} start of slide box motion, t_{11} flap opening trigger, t_{12} start of flap opening, t_{21} airflow reversal trigger, t_{22} start of airflow reversal, t_3*

zero pressure gradient $p_a = p_d$, t_{41} exhaustion trigger, t_{42} start of exhaustion, t_5 end position

6 Landslide Generator Performance

The box position was measured with a cable actuated transducer and a conductive plastic potentiometer (SGG-5000, Pewatron AG). The cable extension sensor had a high frequency response and a low torque, which allowed coping with accelerations up to 6 g and decelerations down to –12 g. The accuracy of the sensor was ±0.5 mm. The box position records of experiments with different parameters are shown in Fig. 8a. All experiments presented herein were conducted with a hill slope angle $\alpha = 45°$. The flap opening was measured with a laser distance sensor (OADM, Baumer Electric AG). The flap-opening angle computed from a secant is shown in Fig. 8b.

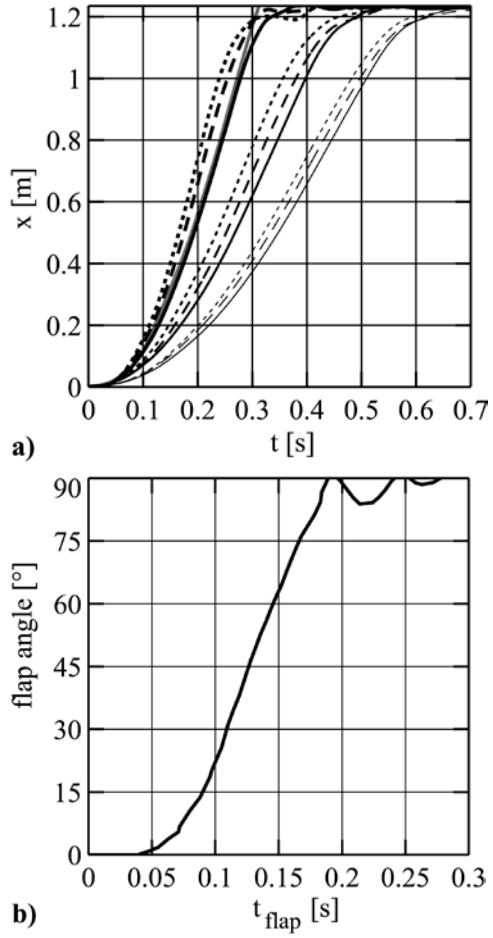

Fig. 8: *a) Slide box position records of experiments with p_a = 8 bar: (——) slide mass m_s = 108 kg, (– –) m_s = 54 kg, (. . . .) m_s = 27 kg; p_a = 3.5 bar: (——) m_s = 108 kg, (– –) m_s = 54 kg, (. . . .) m_s = 27 kg; p_a = 2 bar: (——) m_s = 108 kg, (– –) m_s = 54 kg, (. . . .) m_s = 27 kg; all runs with p_d (t = 0) = 1.3 bar; (——) CACOS-simulation with p_a = 8 bar, p_d (t = 0) = 1.3 bar, m_s = 108 kg, b) Flap opening record with flap opening trigger at $t_{flap} = 0$*

The slide box velocity v_b was derived from the box position record. The high frequency noise was removed from the raw position records prior to first and second derivation. The original signal was denoised with a Daubechies-wavelet transform (Daubechies, 1992; Strang and Nguyen, 1997). Correctly applied wavelet filters do not affect the transient signal whereas conventional filters would weaken the underlying peaks in the signal. The derived box velocity records are shown in Fig. 9a and b. The performance of the pneumatic system strongly depended on the accelerated mass, the pressure gradient and the slope angle. The accelerated mechanical parts had a dead weight m_m = 66 kg including the empty slide box but without the slide load. A maximum box velocity v_B = 7.31 m/s was reached for the slide load m_s = 27 kg at the maximum acceleration pressure p_a = 8 bar. The maximum box velocity decayed to v_B = 6.13 m/s for the slide load m_s = 108 kg at the same pressures. The maximum slide box velocity corresponds to the slide release velocity. The pneumatic system could only be operated for slide release velocities $v_B > 3$ m/s. The minimal slide release velocity v_B = 3 m/s roughly corresponds to the free fall velocity reachable over the acceleration distance of 0.8 m on the hill slope with the angle $\alpha = 45°$.

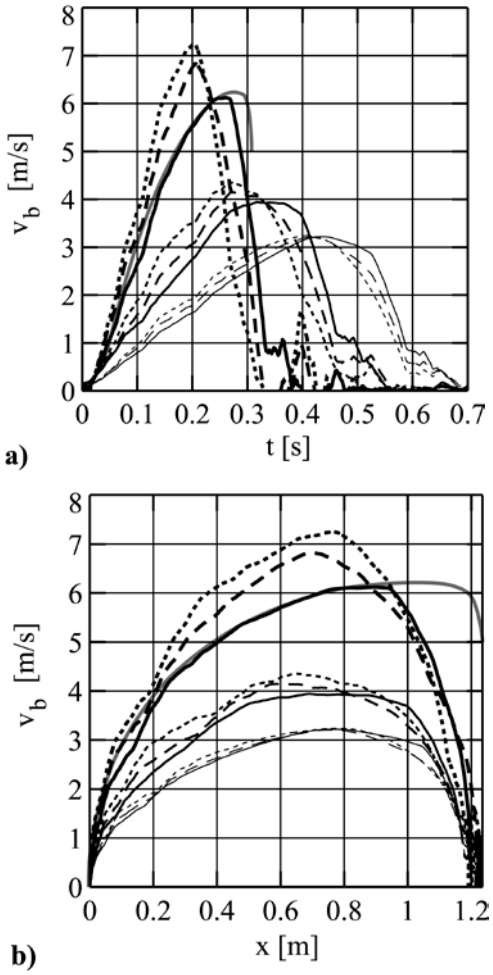

Fig. 9: *Slide box velocity records: a) versus time t and b) versus box position x, notations as in Fig. 8*

The statistical analysis of the maximum slide box velocity v_B was conducted. The sample number was

limited but at least five experimental runs were available for each parameter combination. The mean, minimum and maximum values as well as the standard deviation were computed. The statistical analysis gives insight into the reproducibility of individual experiments. The largest deviations in slide box velocity v_B were within ±5 %. The scattering decreased slightly with increasing acceleration pressure p_a. High acceleration pressures reduced the hysteresis effects in the pneumatic pressure control. The slide release velocity does not correspond to the slide impact velocity.

The slide box acceleration a_b was computed as second derivative from the box position record. The box acceleration records along the linear drives are shown in Fig. 10a. The box accelerations were strongly dependent on the slide mass. Acceleration peaks of 6 g were recorded for the slide load m_s = 27 kg at the maximum acceleration pressure p_a = 8 bar, whereas for m_s = 108 kg the acceleration peaks decayed to 4 g. The characteristic oscillation (peak-trough-double peak) of the acceleration curves was observed at all operating pressures and for all slide loads. Box deceleration peaks of –12 g were reached at impact on the shock absorber at box position 1.085 m. Higher decelerations at best caused damage to the shock absorber as experienced during preliminary testing. The shock absorber and the airflow reversal triggers were adjusted prior to each experiment to avoid higher decelerations.

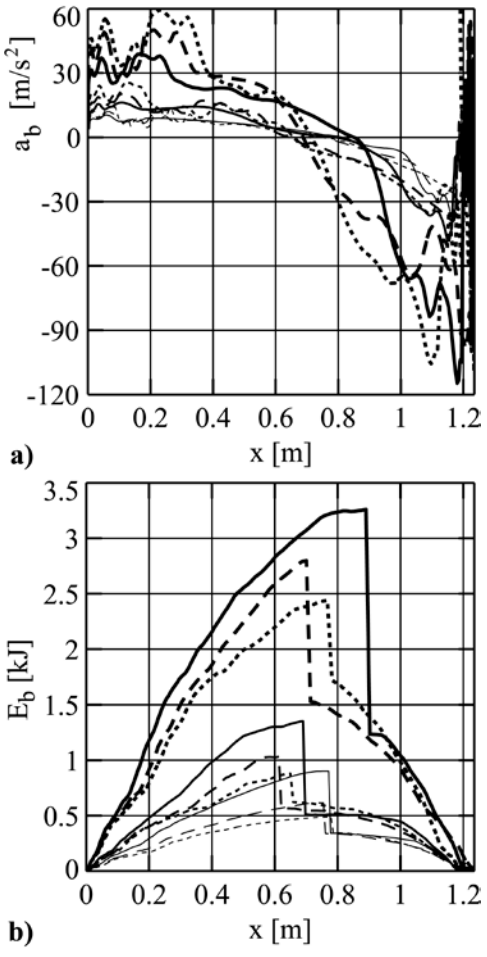

Fig. 10: *a) Slide box acceleration a_b along the linear guides; b) kinetic slide box energy E_b; notations as in Fig. 8*

The evolution of the kinetic box energy along the linear drives is shown in Fig. 10b. The kinetic box energy is determined by

$$E_b = \frac{1}{2} m_b v_b^2 \qquad (1)$$

with the box mass m_b. The discontinuity in the kinetic box energy is due to the slide release at x ($v_b = v_B$). Hence the box mass corresponds to

$$m_b = m_a = m_m + m_s \qquad \forall\, t < t_3 \qquad (2)$$

with the accelerated mass m_a, the fixed mass of the moving mechanical parts m_m = 66 kg, the variable slide mass m_s and the time of the maximum box velocity $t_3 = t$ ($v_b = v_B$). During slide box deceleration the box mass is reduces by the slide release to

$$m_b = m_d = m_m \qquad \forall\, t > t_3 \qquad (3)$$

with the decelerated mass $m_d = m_m$ = 66 kg.

7 Comparison with Calculation and Numerical Simulation

The three main parameters governing the motion behaviour are the pressure difference, the stroke length and the deceleration system. The initial pressure difference, the piston diameter and the moving mass determine the theoretically achievable acceleration. In practical applications the theoretical acceleration is usually not reached due to the friction, the eccentricity of the moving load and the resistance losses of the airflow through the tubes connecting the compressed air reservoirs with the cylinders. The stroke length determines the travel distance available for acceleration and deceleration. The theoretically possible driving force F_a provided by the two pneumatic linear drives under ideal conditions neglecting the influences of both friction and gravity may be computed according to

$$F_a = 2\left(p_a - p_d\right) A_p \qquad (4)$$

resulting in F_a = 6.3 kN with the maximum driving pressure p_a = 8.0 bar in the ventilation chambers, the retaining pressure p_d = 1.3 bar in the exhaust chambers and the piston head area A_p = 5027 mm² determined by the piston diameter d_p = 80 mm. The retaining pressure p_d = 1.3 bar was necessary to hold the loaded slide box in the starting position on the incline with the hill slope angle of 45°. Pre-exhaustion may reduce the retaining pressure to zero and increase the pressure difference $p_a - p_d$ from 6.7 to 8.0 bar. An increase in driving pressure p_a beyond 8.0 bar is not allowed because the cylinders are only certified for 8.0 bar. The theoretical maximum box acceleration is given by

$$a_b = F_a / m_a \qquad (5)$$

with the accelerated mass $m_a = m_m + m_s$. The moving

mechanical mass m_m = 66 kg corresponds to the mass of the pistons, carriages and the slide box. The three slide masses m_s = 27, 54 and 108 kg were investigated. The relationship given by Eq. 5 yields a_b = 68, 53 and 36 m/s^2 with the accelerated masses m_a = 93, 120 and 174 kg. The theoretically reachable maximum box velocity may be computed according to

$$v_B = \sqrt{2\, a_b\, l_a} \tag{6}$$

with the acceleration distance l_a. The relationship given by Eq. 6 yields v_B = 10, 8.9 and 7.3 m/s with an assumed acceleration distance $l_a = 0.6\, l_p$ and the piston accelerations estimated above. The point of zero piston acceleration is ideally located within 50 to 70 % of the stroke length l_p (Sauer, 1996). The calculations overestimate the measured maximum piston velocities v_B = 7.31, 6.72 and 6.13 m/s by 37 to 19 %. The accuracy of the calculation improved with increasing slide mass m_s.

A more accurate prediction of the system behaviour required numerical simulations. The software CACOS version 3.3 was used during project design, optimisation and recalculation. The CACOS (Computer Aided Cylinder Optimisation System) simulation program – developed by Festo Inc. – allows motion sequences to be predicted with variations of the parameters, eliminating complex and expensive trials (Schill, 1993). The entire pneumatic drive system comprising all individual components was designed and parameterised on the graphic user interface. The motion behaviour of all cylinders was simultaneously simulated. The project design was modified according to the simulations in the design stage: the bore diameters at both ends of the cylinders were increased from the standard 12.7 mm to 19.1 mm in order to reach the desired piston velocities of 7 m/s; mechanical over-pressure exhaust valves were added on the rapid exhaust side to avoid pressures beyond 12 bar and damaging the cylinders during the deceleration; an external shock absorber was introduced to dissipate the remaining piston energy. The successful application of the simulation program during the design stage avoided expensive trials.

The comparisons between measurements and numerical simulations are shown in Fig. 8a and Fig. 9 for the case with the highest acceleration pressure p_a = 8 bar and the largest slide mass m_s = 108 kg. The simulated curves are smoother than the measurements, which inevitably contain a certain amount of noise. The numerical simulations closely matched the measurements during the slide box acceleration $t < t_3$, whereas the subsequent slide box deceleration is not predicted correctly. The airflow reversal cannot be simulated in the current version 3.3 of the CACOS software.

8 Conclusions

The developed pneumatic landslide generator enabled the investigation of landslide generated impulse waves in reservoirs, lakes, bays or oceans in a two-dimensional physical laboratory model based on the generalized Froude similarity. The landslides were successfully modelled with a barium-sulphate granulate. The pneumatic landslide generator allowed to control the slide impact characteristics, thus allowing exact reproduction and independent variation of single dynamic slide parameters. In particular different slide impact shapes were produced for the same slide velocity and mass. The two pneumatic linear drives catapulted the slide box with total accelerated masses up to 174 kg on an acceleration distance of less than 0.9 m to velocities up to 7.3 m/s. The linear drives were operated at piston velocities well beyond their certified application range limited to 2 m/s. The slotted cylinders enabled a compact mechanical design and a stroke of 1235 mm on an overall cylinder length of only 1770 mm. The fixed mechanical moving mass of 66 kg after slide release was successfully decelerated from peak velocities up to 7.3 m/s on a deceleration distance of less than 0.6 m down to zero velocity by a temporary airflow and pressure gradient reversal together with an external hydraulic shock absorber. Real time valve response problems were solved with preset trigger signals programmed to the pneumatics control unit according to the determined peak slide box velocity. The behaviour of the whole pneumatic system was simulated with the computer aided cylinder optimisation system software (CACOS). The measurements and numerical simulations showed an excellent agreement on the acceleration part of the stroke, whereas the pneumatic deceleration by the temporary airflow and pressure gradient reversal could not be simulated.

Acknowledgments

The first author would like to express his gratitude towards Prof. Dr. H.-E. Minor, director of VAW, and Prof. Dr. W. H. Hager for their continued advise and support. The presented research work was supported by the Swiss National Science Foundation, grant number 2100-050586.97.

Nomenclature

a_b	Slide box acceleration	[m/s²]
A_p	Piston head cross-section	[m²]
d_p	Piston diameter	[m]
d_g	Grain diameter	[m]
E_b	Slide box energy	[kJ]
F_a	Driving force	[N]
g	Gravitational acceleration	[m/s²]
h	Stillwater depth	[m]
l_a	Acceleration distance	[m]
l_p	Stroke length	[m]
m_a	Accelerated mass	[kg]
m_b	Slide box mass	[kg]
m_d	Decelerated mass	[kg]
m_m	Moving mechanical mass	[kg]
m_s	Slide mass	[kg]
n	Porosity	[-]

p_a	Acceleration pressure	[bar]
p_d	Deceleration pressure	[bar]
s_{box}	Slide thickness in box	[m]
t	Time	[s]
t_{01}	Time of start trigger	[s]
t_{02}	Start of slide box motion	[s]
t_{11}	Time of flap opening trigger	[s]
t_{12}	Start of flap opening	[s]
t_{21}	Time of airflow reversal trigger	[s]
t_{22}	Start of airflow reversal	[s]
t_3	Time of zero pressure gradient	[s]
t_{41}	Time of exhaustion trigger	[s]
t_{42}	Start of exhaustion	[s]
t_5	End of slide box motion	[s]
v_b	Slide box velocity	[m/s]
v_B	Maximum slide box velocity	[m/s]
v_s	Slide release velocity	[m/s]
x	Piston axis coordinate	[m]
α	Hill slope angle	[°]
ρ	Density	[kg/m³]
ρ_g	Grain density	[kg/m³]
ρ_s	Slide density	[kg/m³]

References

Daubechies, I. 1992. *Ten lectures on wavelets*. CBMS-NSF Regional Conference Series in Applied Mathematics, SIAM, Philadelphia.

De Quervain, F. 1980. *Tabellen zum Mineral- und Gesteinsbestimmen, 3rd Edition.* Verlag der Fachvereine VDI, Zürich. (in German)

Fritz, H. M., Hager, W. H. and **Minor, H. - E.** 2001. Lituya Bay case: rockslide impact and wave run-up. *Science of Tsunami Hazards,* Vol. 19(1), pp. 3-22.

Fritz, H. M. 2002a. PIV applied to landslide generated impulse waves. *Laser techniques for fluid mechanics*, selected papers from the 10th International Symposium Lisbon, Portugal July 10-13, eds. Adrian, R. J. et al, Springer, New York 2000, pp. 305-320.

Fritz, H. M. 2002b. *Initial phase of landslide generated impulse waves*. Diss. ETH No. 14'871. Swiss Federal Inst. Techn., Zürich.

Glicken, H. 1996. Rockslide-debris avalanche of May, 18, 1980, Mount St. Helens Volcano. *U.S. Geological Survey Open-File Report,* Washington, pp. 96-677.

Kündig, R., Mumenthaler, T., Eckardt, P., Keusen, H. R., Schindler, C., Hofmann, F., Vogler, R. and **Guntli, P.** 1997. *Die mineralischen Rohstoffe der Schweiz.* Schweizerische Geotechnische Kommission, Zürich. (in German)

Ohmer, M. 1994. Schnelle und langsame Bewegungen mit der Pneumatik. *Pneumatic Tips,* Vol. 39(86), pp. 25-29. (in German)

Sauer, J. 1996. Auf einem Meter: von 0 auf 90 km/h beschleunigen und auf 0 abbremsen. *Pneumatic Tips,* Vol. 41(91), pp. 29-31. (in German)

Schill, M. 1993. Mit CACOS schneller zum Ziel. *Pneumatic/Electronic Tips,* Vol. 38(84), pp. 14-16. (in German)

Slingerland, R. L. and **Voight, B.** 1979. Occurrences, properties and predictive models of landslide-generated impulse waves. Ed. Voight, B. *Developments in geotechnical engineering* 14B, Elsevier, Amsterdam, Rockslides and avalanches 2, pp. 317-397.

Strang, G. and **Nguyen, T.** 1997. *Wavelets and filter banks*. Revised ed., Wellesley-Cambridge Press, Wellesley, Mass.

Tognacca, C. 1999. Beitrag zur Untersuchung der Entstehungsmechanismen von Murgängen. Ed. Minor, H.-E., Versuchsanstalt für Wasserbau, Hydrologie und Glaziologie, ETH Zürich, *VAW-Mitteilung,* Vol. 164. (in German)

Vischer, D. L. and **Hager, W. H.** 1998. *Dam hydraulics*. John Wiley, Chichester.

Hermann M. Fritz
Born on May 20th 1972 in Zürich (Switzerland). Study of Civil Engineering at the Swiss Federal Institute of Technology (ETH) in Zürich. Ph.D.-thesis "Initial phase of landslide generated impulse waves" at the Laboratory of Hydraulics, Hydrology and Glaciology (VAW) of ETH.

Peter Moser
Born on January 21st 1950 in Switzerland. Head of the Division Product and Application Engineering at Festo AG in Dietikon, Switzerland.